



Finite-time coordinated path-following control of leader-following multi-agent systems^{*#}

Weibin CHEN^{†1,3}, Yangyang CHEN^{††1,2}, Ya ZHANG^{1,2}

¹*School of Automation, Southeast University, Nanjing 210096, China*

²*Key Laboratory of Measurement and Control of Complex Systems of Engineering, Ministry of Education, Southeast University, Nanjing 210096, China*

³*Robot Department, Jiangsu Automation Research Institute, Lianyungang 222061, China*

[†]E-mail: jari_chris@163.com; yychen@seu.edu.cn

Received Oct. 5, 2021; Revision accepted Mar. 6, 2022; Crosschecked May 4, 2022; Published online June 15, 2022

Abstract: This paper presents applications of the continuous feedback method to achieve path-following and a formation moving along the desired orbits within a finite time. It is assumed that the topology for the virtual leader and followers is directed. An additional condition of the so-called barrier function is designed to make all agents move within a limited area. A novel continuous finite-time path-following control law is first designed based on the barrier function and backstepping. Then a novel continuous finite-time formation algorithm is designed by regarding the path-following errors as disturbances. The settling-time properties of the resulting system are studied in detail and simulations are presented to validate the proposed strategies.

Key words: Finite-time; Coordinated path-following; Multi-agent systems; Barrier function

<https://doi.org/10.1631/FITEE.2100476>

CLC number: TP24

1 Introduction

Currently, the theory of the formation control problem has emerged as a hot topic and attracted great attention from researchers. To achieve better measurements of biological variables across a range of spatial and temporal scales in the applications in oceanic and planetary explorations (Bertozzi et al., 2005; Fiorelli et al., 2006), unmanned systems are required to simultaneously follow a set of given orbits with a desired formation, which is a special formation control problem called the coordinated path-following control problem.

In the area of coordinated path-following control, many scholars focused on the asymptotic stability of the resulting multi-agent systems. In Cao et al. (2009), a discrete-time consensus-based algorithm was developed to force each follower to track a leader with the desired dynamics, which is also called the consensus tracking control problem. The continuous-time consensus tracking control laws were given in cases of time-invariant formation in Cao and Ren (2012), the time-varying formation in Yu et al. (2018), and the containment motion in Zhang FX and Chen (2022). In Ghabcheloo (2007), a coordinated path-following control law was designed by parameterizing the desired trajectories while synchronizing the orbital parameters. This idea was used in the case of uncertain dynamics in Peng et al. (2013). Noting the geometry of the orbit, a novel geometry extension method was proposed and then integrated into the consensus of the generalized arc-lengths (the

[‡] Corresponding author

^{*} Project supported by the National Natural Science Foundation of China (Nos. 61973074 and 61973082)

[#] Electronic supplementary materials: The online version of this article (<https://doi.org/10.1631/FITEE.2100476>) contains supplementary materials, which are available to authorized users

ORCID: Weibin CHEN, <https://orcid.org/0000-0001-5840-2019>; Yangyang CHEN, <https://orcid.org/0000-0003-0136-0174>

© Zhejiang University Press 2022

smooth functions) to achieve the coordinated path-following task in Zhang FM and Leonard (2007) and Chen and Tian (2015). The geometry extension method was also used to solve the asymptotic coordinated path-following problem with time-varying flows in Chen et al. (2021a, 2021b). However, the coordinated path-following control problem within a finite settling time is still unsolved.

Recently, finite-time control laws in multi-agent systems concentrate on the consensus (or consensus tracking) problems. In Xiao et al. (2009), a finite-time consensus tracking law was designed for a structure that consists of one leader and bidirectional connected followers based on the sliding-mode method. The sliding-mode method was used in the case of directed topologies in Cao et al. (2010) and Wang L and Xiao (2010), in the case of uncertainties in Khoo et al. (2009), and in under-actuated systems in Li TS et al. (2018). The finite-time properties of a sliding-mode-based consensus tracking system can be analyzed using the degree of homogeneity; details can be found in Guan et al. (2012) and Dou et al. (2019). Note that the above control laws are non-smooth and thus sometimes cannot be directly used in actual continuous systems (Qian and Lin, 2001). There is a trend toward designing a continuous finite-time controller for the coordinated control problem. In Li SH et al. (2011), a continuous finite-time consensus law was designed for second-order multi-agent systems under one leader and bidirectional connected followers. A similar idea was designed in Du et al. (2013) using dynamic output feedback. In Huang et al. (2015), an adaptive finite-time consensus algorithm was designed for uncertain nonlinear mechanical systems. The continuous finite-time consensus method was developed to deal with high-order non-holonomic mobile robots with bidirectional topologies in Du et al. (2017) and surface vehicles under the assumption that all followers can access to the leader in Wang N and Li (2020). Note that the objectives of the coordinated path-following control problem include path-following and formation, which are different from those of the consensus problem. It is essential to give a finite-time method to the coordinated path-following problem.

This paper gives a continuous solution to the finite-time control problem of coordinated path-following under directed topologies. To solve the trajectory restriction problem, we present a new bar-

rier function definition that is integrated into backstepping to design a novel continuous finite-time path-following control input projected on the normal vector on the orbit. Another continuous finite-time formation control input projected on the tangential vector on the orbit is designed by regarding the path-following errors as disturbances. Note that the proposed method in this paper is different from our previous adaptive method in Chen et al. (2021b) concerning two conditions: (1) directed networked second-order agents are under consideration and the first-order systems are replaced with bidirectional topologies; (2) a continuous finite-time design method is used to replace the adaptive methods.

2 Preliminaries and problem formulation

2.1 Graph theory and barrier functions

The network topology of the coordinated path-following system can be described by a digraph $\mathcal{G} = \{\mathcal{V}, \mathcal{E}\}$, where nodes $\mathcal{V} = \{\mathcal{V}_0, \mathcal{V}_1, \dots, \mathcal{V}_n\}$ are associated with a virtual leader labeled \mathcal{V}_0 and n vehicles labeled $\mathcal{V}_1, \mathcal{V}_2, \dots, \mathcal{V}_n$, and $\mathcal{E} \subseteq \mathcal{V} \times \mathcal{V}$ is a set of network links. A directed path from node \mathcal{V}_i to node \mathcal{V}_j is a sequence of edges $(\mathcal{V}_i, \mathcal{V}_{i_1}), (\mathcal{V}_{i_1}, \mathcal{V}_{i_2}), \dots, (\mathcal{V}_{i_{l-1}}, \mathcal{V}_{i_l}), (\mathcal{V}_{i_l}, \mathcal{V}_j)$ in the network topology with distinct nodes $\mathcal{V}_{i_k}, k = 1, 2, \dots, l$. A digraph is called a directed tree if there exists a node, called the root, that has directed paths to all the other nodes in the digraph. Let, for $i, j = 0, 1, \dots, n$, $a_{ii} = 0$ and $a_{ij} = 1$ if $(\mathcal{V}_i, \mathcal{V}_j) \in \mathcal{E}$, and $a_{ij} = 0$ otherwise. In addition, define the Laplacian matrix $L \triangleq [l_{ij}]_{i,j=0}^n$ with $l_{ii} = \sum_{j=1}^n a_{ij}$ and $l_{ij} = -a_{ij}$, for any $i \neq j, i, j = 0, 1, \dots, n$.

Assumption 1 The digraph consisting of a virtual leader and n vehicles contains a directed spanning tree with root \mathcal{V}_0 .

For the considered coordinated path-following system, the Laplacian matrix L can be written as

$$L = \begin{bmatrix} 0 & \mathbf{0}_{1 \times n} \\ l_0 & L_1 \end{bmatrix},$$

where $l_0 = [l_{10}, l_{20}, \dots, l_{n0}]^T \in \mathbb{R}^{n \times 1}$ and $L_1 \in \mathbb{R}^{n \times n}$. Suppose that Assumption 1 holds. L_1 is a nonsingular M-matrix and all eigenvalues of L_1 have positive real parts (Zhang Y and Tian, 2009). ρ_{L_1} denotes the smallest eigenvalue of L_1 .

To keep each agent’s trajectory staying in a restricted area when applying the geometry extension method, a new definition of the barrier function Ψ_i is given:

Definition 1 A C^2 function $\Psi_i : (-\varepsilon_i, \varepsilon_i) \rightarrow \mathbb{R}$ is a barrier function with barrier $2\varepsilon_i > 0$ if the following conditions hold:

- (C1) $\lim_{\lambda_i \rightarrow -\varepsilon_i^+} \Psi_i(\lambda_i) = +\infty$ and $\lim_{\lambda_i \rightarrow -\varepsilon_i^+} \nabla \Psi_i(\lambda_i) = -\infty$;
- (C2) $\lim_{\lambda_i \rightarrow \varepsilon_i^-} \Psi_i(\lambda_i) = +\infty$ and $\lim_{\lambda_i \rightarrow \varepsilon_i^-} \nabla \Psi_i(\lambda_i) = +\infty$;
- (C3) $\nabla \Psi_i(0) = 0$;
- (C4) $|\nabla \Psi_i| \geq c_\Psi |\lambda_i|$ with a bounded positive constant c_Ψ .

Remark 1 The barrier function in Definition 1 is different from those in traditional definitions, because condition (C4) is added and used to yield the finite-time convergence of the resulting system with the state constraint $\Omega_i = \{p_i \in \mathbb{R}^2 \mid |\lambda_i(p_i(t))| < \varepsilon_i\}$. It is noted that the additional condition (C4) is not difficult to satisfy in traditional barrier functions. For example,

$$\Psi(\lambda_i) = \int_{\lambda_{i0}}^{\lambda_i} \left[c_1 \left(\frac{1}{\varepsilon_i - \tau} - \frac{1}{\varepsilon_i + \tau} \right) + c_2 (\ln(\varepsilon_i + \tau) - \ln(\varepsilon_i - \tau)) \right] d\tau, \tag{1}$$

where c_1 and c_2 are positive constants. In this case, one can select parameter c_2 from 0.3 to 0.8 to yield condition (C4), as shown in Fig. 1.

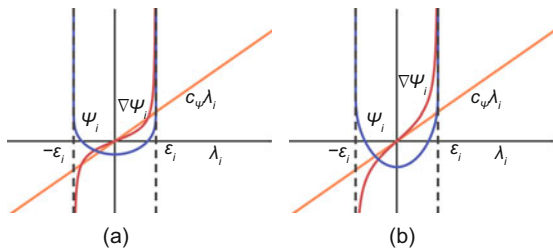


Fig. 1 Sketches of Ψ_i , $\nabla \Psi_i$, and $c_\Psi \lambda_i$ with respect to different c_2 values: (a) $c_2 = 0.3$; (b) $c_2 = 0.8$ ($c_\Psi = 0.7$, $\varepsilon_i = 2$, and $c_1 = 0.2$)

2.2 Some lemmas

Lemma 1 (Chen and Tian, 2015) Consider any simple, closed, and regular orbit satisfying the following conditions:

- (C5) $\|\mathcal{C}_{i0}(\phi_i)\| > \varepsilon \geq 0$;
- (C6) $0 < \varepsilon \leq \left\| \frac{d\mathcal{C}_{i0}(\phi_i)}{d\phi_i} \right\| < +\infty$;
- (C7) $\left| \mathcal{C}_{i0}(\phi_i), \frac{d\mathcal{C}_{i0}(\phi_i)}{d\phi_i} \right| \neq 0$.

Identifying the orbit by map \mathcal{C}_{i0} , there exists a constant $\varepsilon_i > 0$ such that $\mathcal{C}_{i(\cdot)}(\cdot, \cdot)$ is a diffeomorphism on $[0, 2\pi) \times (-\varepsilon_i, \varepsilon_i)$. Moreover, there exists an open set $\Omega_i \subset \mathbb{R}^2$, which is a tubular neighborhood of the orbit, and a smooth function $\lambda_i : \Omega_i \rightarrow (-\varepsilon_i, \varepsilon_i)$, which is called the orbit function (its value is called the orbit value), such that the following conditions hold:

- (C8) $\|\nabla \lambda_i\| = \left\| \frac{\partial \lambda_i}{\partial p_i} \right\| \neq 0$, for all $p_i \in \Omega_i$;
- (C9) $\lambda_i(p_i) = c$, for all points p_i on the orbit identified by \mathcal{C}_{ic} with $c \in (-\varepsilon_i, \varepsilon_i)$.

\mathcal{C}_{ic} is a level line of the orbit function $\lambda_i(p_i)$, and the orbit value associated with orbit \mathcal{C}_{i0} is zero.

Definition 2 (Chen et al., 2021a) The generalized arc-lengths ξ_i are C^1 functions of the arc-lengths s_i and $\left| \frac{\partial \xi_i}{\partial s_i} \right| \geq c_\xi > 0$.

Lemma 2 (Chen et al., 2021a) The C^1 invertible mappings $\xi_i : \mathbb{R} \rightarrow \mathbb{R}$ define a change of coordinates, which allows formulation of the coordinated path-following problem with state variables s_i into the consensus problem described by

$$\lim_{t \rightarrow \infty} (\xi_i(t) - \xi_0(t)) = 0, \tag{2}$$

with state variables $\xi_i(s_i)$. To form the desired formation, the desired arc-length s_i^* of the i^{th} follower is determined by the arc-length of the leader s_0 via $s_i^* = g_{s_i s_0}(s_0)$, where $g_{s_i s_0} : \mathbb{R} \rightarrow \mathbb{R}$ is an invertible mapping explicitly defined by the desired formation. By Eq. (2), ξ_0 and ξ_i are such that

$$\xi_i(s_i^*) = \xi_0(s_0).$$

Note that $s_0 = g_{s_i s_0}^{-1}(s_i^*)$ yields $\xi_i = \xi_0 \circ g_{s_i s_0}^{-1}$, which properly defines ξ_i for any given ξ_0 , since $g_{s_i s_0}$ is known. Here, “ \circ ” is the symbol for composition of functions; that is, ξ_i is the composition of ξ_0 and $g_{s_i s_0}^{-1}$.

2.3 Problem formulation

In this study, we first consider the cases of static virtual leader and dynamic virtual leader. In a fixed inertial reference frame, the model of the static virtual leader is the first-order dynamics such that $\dot{p}_0 = 0$, where $p_0 = [p_{x_0}, p_{y_0}]^T \in \mathbb{R}^2$ is its position. For $i = 1, 2, \dots, n$, the dynamic equation for the

i^{th} follower satisfying the second-order dynamics is given by

$$\begin{cases} \dot{p}_i = v_i, \\ \dot{v}_i = u_i, \end{cases} \quad (3)$$

where $p_i = [p_{x_i}, p_{y_i}]^T \in \mathbb{R}^2$ and $v_i = [v_{x_i}, v_{y_i}]^T \in \mathbb{R}^2$ denote the position and velocity, respectively. $u_i = [u_{x_i}, u_{y_i}]^T \in \mathbb{R}^2$ denotes the control input.

Suppose that the desired orbit associated with each agent is a simple, closed, and regular curve with nonzero curvature. According to Lemma 1, this curve can be extended geometrically to a set of level curves, which can be defined by a smooth function (the orbit function) $\lambda_i : \Omega_i \rightarrow (-\varepsilon_i, \varepsilon_i)$; the desired orbit can be defined by $\lambda_i(p_i) = 0$, where $\Omega_i \subset \mathbb{R}^2$ is an open set and $p_i \in \mathbb{R}^2$.

The path-following error can be described by the value of the orbit function and the path-following task is achieved if

$$\lim_{t \rightarrow T} \lambda_i(p_i(t)) = 0, \quad (4)$$

with a finite time $T > 0$ and $p_i(t) \in \Omega_i$, for all $t \geq 0$, where

$$\Omega_i = \{p_i \in \mathbb{R}^2 \mid |\lambda_i(p_i(t))| < \varepsilon_i\}. \quad (5)$$

Let the arc-lengths be given by

$$s_i(\lambda_i, \phi_i) \triangleq \int_{\phi_i^*}^{\phi_i} \frac{\partial s_i(\lambda_i, \tau)}{\partial \tau} d\tau, \quad (6)$$

where ϕ_i^* is the parameter associated with the starting point of the arc of s_i . The generalized arc-lengths $\xi_i : \mathbb{R} \rightarrow \mathbb{R}$ of s_i are used to describe the formation along the curves. $\partial \xi_i / \partial s_i$ is a constant and satisfies $c_{\underline{\xi}} \leq |\partial \xi_i / \partial s_i| \leq c_{\bar{\xi}}$ with two positive constants $c_{\underline{\xi}}$ and $c_{\bar{\xi}}$. From Lemma 2, the task of achieving coordinate formation in finite time T can be described as follows:

$$\lim_{t \rightarrow T} \xi_i(t) = \xi_0. \quad (7)$$

The finite-time coordinated path-following control problem is as follows: For $i = 1, 2, \dots, n$, consider system (3) and the initial position $p_i(0) \in \Omega_i$. Suppose that Assumption 1 holds. Design a finite-time coordinated path-following control u_i such that the closed-loop system satisfies Eqs. (4) and (7).

Remark 2 The discontinuous laws based on $\text{sgn}(\cdot)$ (Khoo et al., 2009; Xiao et al., 2009; Cao et al., 2010;

Wang L and Xiao, 2010; Guan et al., 2012; Li TS et al., 2018; Dou et al., 2019) might cause signal chattering in the closed-loop system. In practice, it is difficult to accomplish these discontinuous laws.

Remark 3 This paper is devoted to designing a continuous finite-time control law for directed networking second-order agents for the coordinated path-following problem. However, Chen et al. (2021b) dealt with the adaptive design for first-order agents with unknown time-varying parameters and bidirectional topologies.

3 Main results

In this study, we first consider the cases of static virtual leader and dynamic virtual leader. The design precedence is as follows: (1) decouple the whole system as a path-following subsystem and a formation subsystem; (2) regard v_{N_i} as a virtual controller \hat{v}_{N_i} and design u_{N_i} by backstepping to achieve finite-time path-following along the given orbits (Theorem 1); (3) regard v_{T_i} as a virtual controller \hat{v}_{T_i} and design u_{T_i} by backstepping to achieve finite-time formation along the given orbits (Theorem 2); (4) according to Theorems 1 and 2, give Theorem 3 to show the finite-time convergence of the coordinated path-following control system. Then a corollary is given to show the case of the dynamic virtual leader.

Section 3.1 gives the open-loop system (i.e., the error equations of the coordinated path-following control system), which is used to design the path-following control law in Section 3.2 and the formation control law in Section 3.3.

3.1 Open-loop system

By differentiating λ_i , the path-following dynamics of agent i is obtained as follows:

$$\dot{\lambda}_i = \|\nabla \lambda_i\| v_{N_i}, \quad (8)$$

where $v_{N_i} = N_i^T v_i$ denotes the velocity projected on vector N_i which is normal to the level orbit of the current position of agent i and $N_i = \frac{\nabla \lambda_i}{\|\nabla \lambda_i\|}$. Differentiating both sides of v_{N_i} yields

$$\dot{v}_{N_i} = u_{N_i} + \Delta_{N_i}, \quad (9)$$

where $u_{N_i} = N_i^T u_i$ denotes the control input projected on the normal vector N_i , $\Delta_{N_i} = v_i^T \dot{N}_i$, and $\dot{N}_i = \frac{(\nabla^2 \lambda_i) v_i}{\|\nabla \lambda_i\|} - \frac{N_i N_i^T (\nabla^2 \lambda_i) v_i}{\|\nabla \lambda_i\|}$.

Let T_i denote the vector which is tangent to the level orbit of the current position of agent i and $T_i = R^T N_i = [R_1, R_2]^T N_i$, where $R_1 = [0, 1]^T$ and $R_2 = [-1, 0]^T$. Then the dynamics of ξ_i is given by

$$\dot{\xi}_i = \frac{\partial \xi_i}{\partial s_i} v_{T_i} + \Delta_{\xi_i}, \quad (10)$$

where $v_{T_i} = T_i^T v_i$ and $\Delta_{\xi_i} = \frac{\partial \xi_i}{\partial s_i} \frac{\partial s_i}{\partial \lambda_i} \|\nabla \lambda_i\| v_{N_i}$. The proof of Eq. (10) is provided in the supplementary materials. Differentiating both sides of v_{T_i} yields

$$\dot{v}_{T_i} = u_{T_i} + \Delta_{T_i}, \quad (11)$$

where $u_{T_i} = T_i^T u_i$ denotes the control input projected on the tangent vector N_i and $\Delta_{T_i} = R^T \dot{N}_i v_i$.

Let $\varsigma_i = \sum_{j=0}^n a_{ij} (\xi_i - \xi_j)$ denote the formation errors. The dynamics of ς_i is described by

$$\dot{\varsigma}_i = \sum_{j=0}^n a_{ij} \left(\frac{\partial \xi_i}{\partial s_i} v_{T_i} + \Delta_{\xi_i} - \frac{\partial \xi_j}{\partial s_j} v_{T_j} - \Delta_{\xi_j} \right). \quad (12)$$

As a result, the equations of the formation tracking control system are given by Eqs. (8), (9), (11), and (12).

3.2 Path-following controller design

Let us first consider the path-following subsystem consisting of Eqs. (8) and (9) and let the virtual control \hat{v}_{N_i} be

$$\hat{v}_{N_i} = -k_1 (\nabla \Psi_i)^{\frac{1}{\alpha}}, \quad (13)$$

where $1 \leq \alpha = \frac{p_1}{p_2}$, p_1 and p_2 are positive odd integers, and the control gain k_1 will be selected later. Consider the path-following candidate Lyapunov function as

$$V_P = \sum_{i=1}^n \Psi_i(\lambda_i) + \gamma_1 \sum_{i=1}^n \int_{\hat{v}_{N_i}}^{v_{N_i}} (\tau^\alpha - \hat{v}_{N_i}^\alpha)^{2-\frac{1}{\alpha}} d\tau, \quad (14)$$

where $\gamma_1 = \frac{1}{(2-\frac{1}{\alpha})k_1^{1+\alpha}}$. The first term on the right-hand side of Eq. (14) contributes to achieving the path-following objective, i.e., Eq. (4). The second term contributes to guaranteeing the convergence of the differences $\bar{v}_{N_i} = v_{N_i}^\alpha - \hat{v}_{N_i}^\alpha$. Let $\tilde{v}_{N_i} = v_{N_i} - \hat{v}_{N_i}$. Differentiating both sides of Eq. (14) along the

trajectories of Eqs. (8), (9), and (13) yields

$$\begin{aligned} \dot{V}_P \leq & \sum_{i=1}^n \|\nabla \lambda_i\| |\nabla \Psi_i \tilde{v}_{N_i}| - \sum_{i=1}^n k_1 \|\nabla \lambda_i\| (\nabla \Psi_i)^{1+\frac{1}{\alpha}} \\ & + \gamma_1 \sum_{i=1}^n \bar{v}_{N_i}^{2-\frac{1}{\alpha}} (u_{N_i} + \Delta_{N_i}) + f_P, \end{aligned} \quad (15)$$

where

$$f_P = \sum_{i=1}^n k_1^{-1} \|\nabla \lambda_i\| |\nabla^2 \Psi_i| |\bar{v}_{N_i}|^{1-\frac{1}{\alpha}} |v_{N_i}| |\tilde{v}_{N_i}|.$$

The proof of inequality (15) is provided in the supplementary materials.

Since $|\tilde{v}_{N_i}| = \left| (v_{N_i}^\alpha)^{\frac{1}{\alpha}} - (\hat{v}_{N_i}^\alpha)^{\frac{1}{\alpha}} \right|$, according to Lemmas A.1 and A.2 in Qian and Lin (2001), we have

$$\begin{cases} |\tilde{v}_{N_i}| \leq 2^{1-\frac{1}{\alpha}} |v_{N_i}^\alpha - \hat{v}_{N_i}^\alpha|^{\frac{1}{\alpha}}, \\ |\nabla \Psi_i \tilde{v}_{N_i}| \leq |\nabla \Psi_i|^{1+\frac{1}{\alpha}} + c_{\phi_1} |\bar{v}_{N_i}|^{1+\frac{1}{\alpha}}, \\ |\bar{v}_{N_i}| |\nabla \Psi_i|^{\frac{1}{\alpha}} \leq |\nabla \Psi_i|^{1+\frac{1}{\alpha}} + c_{\phi_2} |\bar{v}_{N_i}|^{1+\frac{1}{\alpha}}, \end{cases} \quad (16)$$

where $\phi_1 = 2^{-1-\frac{1}{\alpha}}(1+\alpha)/\alpha$, $\phi_2 = 1+\alpha$, $c_{\phi_1} = 2^{-1-\frac{1}{\alpha}}\phi_1^{-\alpha}/(1+\alpha)$, and $c_{\phi_2} = \phi_2^{-\frac{1}{\alpha}}\alpha/(1+\alpha)$.

The proof of inequality (16) is provided in the supplementary materials.

Note that $|v_{N_i}| |\tilde{v}_{N_i}| \leq |\hat{v}_{N_i}| |\tilde{v}_{N_i}| + |\tilde{v}_{N_i}|^2$. From Eq. (13) and inequality (16), we can conclude that

$$\begin{aligned} f_P \leq & \sum_{i=1}^n k_1^{-1} \|\nabla \lambda_i\| |\nabla^2 \Psi_i| \left[2^{2-\frac{2}{\alpha}} |\bar{v}_{N_i}|^{1+\frac{1}{\alpha}} \right. \\ & \left. + k_1 2^{1-\frac{1}{\alpha}} \left(|\nabla \Psi_i|^{1+\frac{1}{\alpha}} + c_{\phi_2} |\bar{v}_{N_i}|^{1+\frac{1}{\alpha}} \right) \right]. \end{aligned} \quad (17)$$

On the set $\Phi_P = \{(\lambda_i, \tilde{v}_{N_i}) | V_P \leq c_P\}$, for some $c_P > 0$, one has $c_{\underline{\lambda}} \leq \|\nabla \lambda_i\| \leq c_{\bar{\lambda}}$ and $|\nabla^2 \Psi_i| \leq c_{\Psi^2}$ with some $c_{\underline{\lambda}} > 0$, $c_{\bar{\lambda}} > 0$, and $c_{\Psi^2} > 0$. Exploiting inequalities (16) and (17), we conclude that

$$\begin{aligned} \dot{V}_P \leq & \gamma_1 \sum_{i=1}^n \bar{v}_{N_i}^{2-\frac{1}{\alpha}} (u_{N_i} + \Delta_{N_i}) + \sum_{i=1}^n c_{P2} \bar{v}_{N_i}^{1+\frac{1}{\alpha}} \\ & - \sum_{i=1}^n \left(k_1 c_{\underline{\lambda}} - c_{P1} \right) (\nabla \Psi_i)^{1+\frac{1}{\alpha}}, \end{aligned} \quad (18)$$

which yields

$$u_{N_i} = -\Delta_{N_i} - k_2 \bar{v}_{N_i}^{-1+\frac{2}{\alpha}}, \quad (19)$$

where

$$\begin{cases} k_1 > c_{\underline{\lambda}}^{-1} (c_{P1} + \beta_{P1}), \\ k_2 > \left(2 - \frac{1}{\alpha}\right) k_1^{1+\alpha} (c_{P2} + \beta_{P1}). \end{cases}$$

Herein, $c_{P1} = c_{\tilde{\lambda}} + c_{\tilde{\lambda}} 2^{1-\frac{1}{\alpha}} c_{\Psi^2}$, $c_{P2} = c_{\tilde{\lambda}} \left(c_{\phi_1} + k_1^{-1} 2^{2-\frac{2}{\alpha}} c_{\Psi^2} + 2^{1-\frac{1}{\alpha}} c_{\phi_2} c_{\Psi^2} \right)$, and β_{P1} is an arbitrary positive constant. Note that

$$(\nabla\Psi_i)^{1+\frac{1}{\alpha}} + \tilde{v}_{N_i}^{1+\frac{1}{\alpha}} \geq \left((\nabla\Psi_i)^2 + \tilde{v}_{N_i}^2 \right)^{(1+\frac{1}{\alpha})/2}. \tag{20}$$

The proof of inequality (18) is provided in the supplementary materials.

Suppose that $V_P(t) \neq 0$. Substituting Eq. (19) into inequality (18) yields

$$\begin{aligned} \dot{V}_P &\leq -\beta_{P1} \sum_{i=1}^n \left((\nabla\Psi_i)^2 + \tilde{v}_{N_i}^2 \right)^{(1+\frac{1}{\alpha})/2} \\ &= -g_P V_P^{(1+\frac{1}{\alpha})/2}, \end{aligned} \tag{21}$$

where $g_P = \beta_{P1} V_P^{-(1+\frac{1}{\alpha})/2} \sum_{i=1}^n \left((\nabla\Psi_i)^2 + \tilde{v}_{N_i}^2 \right)^{(1+\frac{1}{\alpha})/2}$. By Eq. (19), the closed-loop equation associated with the path-following subsystem for the i^{th} follower is

$$\begin{cases} \dot{\lambda}_i = -k_1 \|\nabla\lambda_i\| (\nabla\Psi_i)^{\frac{1}{\alpha}} + \|\nabla\lambda_i\| \tilde{v}_{N_i}, \\ \dot{\tilde{v}}_{N_i} = -\alpha v_{N_i}^{\alpha-1} k_2 \tilde{v}_{N_i}^{\frac{2}{\alpha}-1} - \dot{v}_{N_i}^{\alpha}. \end{cases} \tag{22}$$

Remark 4 It is obvious that the closed-loop system (22) for path-following is not homogeneous. Therefore, the finite-time stability analysis methods given in Guan et al. (2012) and Dou et al. (2019) cannot be applied in this study.

Note that $0 < (1 + \frac{1}{\alpha})/2 < 1$. To apply Theorem 4.2 in Bhat and Bernstein (2000) (which is provided in the supplementary materials), we will show that g_P has a lower bound. From condition (C4), we have

$$\begin{cases} \Psi_i = \int_{\lambda_{i0}}^{\lambda_i} \nabla\Psi_i(\tau) d\tau \leq c_{\Psi}^{-1} |\nabla\Psi_i|^2 + |\nabla\Psi_i| \varepsilon_i, \\ \int_{\tilde{v}_{N_i}}^{v_{N_i}} (\tau^{\alpha} - \hat{v}_{N_i}^{\alpha})^{2-\frac{1}{\alpha}} d\tau \leq 2^{1-\frac{1}{\alpha}} |v_{N_i}^{\alpha} - \hat{v}_{N_i}^{\alpha}|^2, \end{cases}$$

with $\lambda_{i0} = \lambda_i(0)$, which yields

$$V_P \leq \beta_{P3} \sum_{i=1}^n \left[(\nabla\Psi_i)^2 + (v_{N_i}^{\alpha} - \hat{v}_{N_i}^{\alpha})^2 \right] + c_{P3}, \tag{23}$$

where $\beta_{P3} = \max \left\{ c_{\Psi}^{-1}, \frac{2^{1-\frac{1}{\alpha}}}{(2-\frac{1}{\alpha})k_1^{1+\alpha}} \right\}$ and $c_{P3} =$

$\sum_{i=1}^n |\nabla\Psi_i| \varepsilon_i$. As a result, we have

$$\begin{aligned} g_P &\geq \frac{\beta_{P1} \sum_{i=1}^n \left((\nabla\Psi_i)^2 + \tilde{v}_{N_i}^2 \right)^{(1+\frac{1}{\alpha})/2}}{\left(\beta_{P3} \sum_{i=1}^n \left((\nabla\Psi_i)^2 + \tilde{v}_{N_i}^2 \right) + c_{P3} \right)^{(1+\frac{1}{\alpha})/2}} \\ &\geq \beta_{P4}, \end{aligned} \tag{24}$$

where β_{P4} is positive and bounded. According to Theorem 4.2 in Bhat and Bernstein (2000), we establish the following theorem:

Theorem 1 Suppose that the initial positions of vehicles are such that $p_i(0) \in \Omega_i$. Assume moreover that Assumption 1 holds. Then the path-following objective (Eq. (4)) can be achieved by the finite-time control u_{N_i} given in Eq. (19), for $i = 1, 2, \dots, n$.

Proof From inequality (21), we conclude that the function V_P is bounded all the time, which implies that the objective (Eq. (5)) is satisfied according to conditions (C1) and (C2). From inequalities (21) and (24), we conclude that $\lambda_i = 0$ and that \tilde{v}_{N_i} ($i = 1, 2, \dots, n$) are the finite-time stable equilibria of the closed-loop path-following subsystem (22).

3.3 Coordinated formation controller design

In the following, we will consider the formation subsystem consisting of Eqs. (11) and (12). Let the virtual control \hat{v}_{T_i} be

$$\hat{v}_{T_i} = - \left(\frac{\partial \xi_i}{\partial s_i} \right)^{-1} k_3 s_i^{\frac{1}{\alpha}}, \tag{25}$$

where k_3 is a positive control gain and will be selected later. Consider the coordinated formation candidate Lyapunov function as

$$V_F = \frac{1}{2} \sum_{i=1}^n s_i^2 + \gamma_2 \sum_{i=1}^n \int_{\hat{v}_{T_i}}^{v_{T_i}} (\tau^{\alpha} - \hat{v}_{T_i}^{\alpha})^{2-\frac{1}{\alpha}} d\tau, \tag{26}$$

where $\gamma_2 = \frac{1}{(2-\frac{1}{\alpha})k_3^{1+\alpha}}$. In Eq. (26), the first term on the right-hand side contributes to achieving the formation objective, i.e., Eq. (7), and the second term contributes to guaranteeing the convergence of the differences $\tilde{v}_{T_i} = v_{T_i}^{\alpha} - \hat{v}_{T_i}^{\alpha}$. Let $\tilde{v}_{T_i} = v_{T_i} - \hat{v}_{T_i}$. Differentiating both sides of Eq. (26) along the

trajectories of Eqs. (11), (12), and (25) yields

$$\begin{aligned} \dot{V}_F = & -k_3 \sum_{i=1}^n \varsigma_i \sum_{j=0}^n a_{ij} \left(\varsigma_i^{\frac{1}{\alpha}} - \varsigma_j^{\frac{1}{\alpha}} \right) + f_F \\ & + \gamma_2 \sum_{i=1}^n \bar{v}_{T_i}^{2-\frac{1}{\alpha}} (u_{T_i} + \Delta_{T_i}) + g_{F1} + g_{F2}, \end{aligned} \quad (27)$$

where

$$f_F = \sum_{i=1}^n \varsigma_i \sum_{j=0}^n a_{ij} \left(\frac{\partial \xi_i}{\partial s_i} \bar{v}_{T_i} - \frac{\partial \xi_j}{\partial s_j} \bar{v}_{T_j} \right), \quad (28)$$

$$g_{F1} = \sum_{i=1}^n \varsigma_i \sum_{j=0}^n a_{ij} \left(\Delta_{\xi_i} - \Delta_{\xi_j} \right), \quad (29)$$

$$\begin{aligned} g_{F2} = & \frac{1}{k_3} \sum_{i=1}^n \left(\frac{\partial \xi_i}{\partial s_i} \right)^{-\alpha} \int_{\hat{v}_{T_i}}^{v_{T_i}} (\tau^\alpha - \hat{v}_{T_i}^\alpha)^{1-\frac{1}{\alpha}} d\tau \\ & \cdot \sum_{j=0}^n a_{ij} \left(\frac{\partial \xi_i}{\partial s_i} v_{T_i} + \Delta_{\xi_i} - \frac{\partial \xi_j}{\partial s_j} v_{T_j} - \Delta_{\xi_j} \right). \end{aligned} \quad (30)$$

The proof of Eq. (27) is provided in the supplementary materials.

Note that

$$f_F \leq \sum_{i=1}^n |\varsigma_i| \left(\gamma_3 c_{\xi} |\bar{v}_{T_i}| + \gamma_4 c_{\xi} \sum_{j=0}^n |\bar{v}_{T_j}| \right), \quad (31)$$

where $\gamma_3 = \max_{\forall i} \left\{ \sum_{j=0}^n a_{ij} \right\}$ and $\gamma_4 = \max_{\forall i,j} \{a_{ij}\}$. From Lemmas A.1 and A.2 in Qian and Lin (2001), we have

$$\begin{cases} |\bar{v}_{T_i}| \leq 2^{1-\frac{1}{\alpha}} |v_{T_i}^\alpha - \hat{v}_{T_i}^\alpha|^{\frac{1}{\alpha}}, \\ |\varsigma_i| |\bar{v}_{T_i}| \leq |\varsigma_i|^{1+\frac{1}{\alpha}} + c_{F1} |v_{T_i}^\alpha - \hat{v}_{T_i}^\alpha|^{1+\frac{1}{\alpha}}, \\ |\varsigma_i| |\bar{v}_{T_j}| \leq |\varsigma_i|^{1+\frac{1}{\alpha}} + c_{F1} |v_{T_j}^\alpha - \hat{v}_{T_j}^\alpha|^{1+\frac{1}{\alpha}}, \end{cases} \quad (32)$$

where $c_{F1} = 2^{-1-\frac{1}{\alpha}} \phi_{F1}^{-\alpha} / (1 + \alpha)$ and $\phi_{F1} = 2^{-1-\frac{1}{\alpha}} (1 + \alpha) / \alpha$. Substituting inequality (32) into inequality (31) yields

$$f_F \leq c_{\sigma 1} \sum_{i=1}^n |\varsigma_i|^{1+\frac{1}{\alpha}} + c_{vT1} \sum_{j=0}^n |\bar{v}_{T_j}|^{1+\frac{1}{\alpha}}, \quad (33)$$

where $c_{\sigma 1} = \gamma_3 c_{\xi} + (n + 1) \gamma_4 c_{\xi}$ and $c_{vT1} = \gamma_3 c_{\xi} c_{F1} + n \gamma_4 c_{\xi} c_{F1}$. Note that

$$g_{F2} \leq g_{F21} + g_{F22}, \quad (34)$$

where

$$\begin{cases} g_{F21} = \sum_{i=1}^n k_3^{-1} c_{\xi}^{-\alpha} |v_{T_i}^\alpha - \hat{v}_{T_i}^\alpha|^{1-\frac{1}{\alpha}} |v_{T_i} - \hat{v}_{T_i}| \\ \quad \cdot \sum_{j=0}^n a_{ij} \left| \frac{\partial \xi_i}{\partial s_i} v_{T_i} - \frac{\partial \xi_j}{\partial s_j} v_{T_j} \right|, \\ g_{F22} = \sum_{i=1}^n k_3^{-1} c_{\xi}^{-\alpha} |v_{T_i}^\alpha - \hat{v}_{T_i}^\alpha|^{1-\frac{1}{\alpha}} |v_{T_i} - \hat{v}_{T_i}| \\ \quad \cdot \sum_{j=0}^n a_{ij} \left| \Delta_{\xi_i} - \Delta_{\xi_j} \right|. \end{cases} \quad (35)$$

Due to the fact that

$$\begin{cases} |v_{T_i}| |v_{T_i} - \hat{v}_{T_i}| \leq |\bar{v}_{T_i}|^2 + |\hat{v}_{T_i}| |\bar{v}_{T_i}|, \\ |v_{T_j}| |v_{T_i} - \hat{v}_{T_i}| \leq |\bar{v}_{T_j}| |\bar{v}_{T_i}| + |\hat{v}_{T_j}| |\bar{v}_{T_i}|, \end{cases} \quad (36)$$

from Eq. (25), inequality (32), and Eq. (35), one has

$$\begin{aligned} g_{F21} \leq & \sum_{i=1}^n \left(c_{g1} |\bar{v}_{T_i}|^{1+\frac{1}{\alpha}} + c_{g2} |\varsigma_i|^{\frac{1}{\alpha}} |\bar{v}_{T_i}| \right) \\ & + \sum_{i=1}^n \sum_{j=0}^n \left(c_{g3} |\bar{v}_{T_j}|^{\frac{1}{\alpha}} |\bar{v}_{T_i}| + c_{g4} |\varsigma_j|^{\frac{1}{\alpha}} |\bar{v}_{T_i}| \right), \end{aligned} \quad (37)$$

where $c_{g1} = k_3^{-1} c_{\xi}^{-\alpha} \gamma_3 c_{\xi} 2^{2-\frac{2}{\alpha}}$, $c_{g2} = c_{\xi}^{-\alpha-1} \gamma_3 c_{\xi} 2^{1-\frac{1}{\alpha}}$, $c_{g3} = k_3^{-1} c_{\xi}^{-\alpha} \gamma_4 c_{\xi} 2^{2-\frac{2}{\alpha}}$, and $c_{g4} = c_{\xi}^{-\alpha-1} \gamma_4 c_{\xi} 2^{1-\frac{1}{\alpha}}$.

The proof of inequality (37) is provided in the supplementary materials.

From Lemmas A.1 and A.2 in Qian and Lin (2001), we have

$$\begin{cases} |\varsigma_i|^{\frac{1}{\alpha}} |\bar{v}_{T_i}| \leq |\varsigma_i|^{1+\frac{1}{\alpha}} + c_{F2} |\bar{v}_{T_i}|^{1+\frac{1}{\alpha}}, \\ |\varsigma_j|^{\frac{1}{\alpha}} |\bar{v}_{T_i}| \leq |\varsigma_j|^{1+\frac{1}{\alpha}} + c_{F2} |\bar{v}_{T_i}|^{1+\frac{1}{\alpha}}, \\ |\bar{v}_{T_j}|^{\frac{1}{\alpha}} |\bar{v}_{T_i}| \leq |\bar{v}_{T_j}|^{1+\frac{1}{\alpha}} + c_{F2} |\bar{v}_{T_i}|^{1+\frac{1}{\alpha}}, \end{cases} \quad (38)$$

with $c_{F2} = \alpha \phi_{F2}^{-\frac{1}{\alpha}} / (1 + \alpha)$ and $\phi_{F2} = 1 + \alpha$, which yields

$$g_{F21} \leq c_{vT2} \sum_{i=1}^n |\bar{v}_{T_i}|^{1+\frac{1}{\alpha}} + c_{\sigma 2} \sum_{i=1}^n |\varsigma_i|^{1+\frac{1}{\alpha}}, \quad (39)$$

where $c_{vT2} = c_{g1} + c_{g2} c_{F2} + n c_{g3} + n c_{g3} c_{F2} + n c_{g4} c_{F2}$ and $c_{\sigma 2} = c_{g2} + n c_{g4}$.

From inequalities (34) and (39), we have

$$g_{F2} \leq c_{vT2} \sum_{i=1}^n |\bar{v}_{T_i}|^{1+\frac{1}{\alpha}} + c_{\sigma 2} \sum_{i=1}^n |\varsigma_i|^{1+\frac{1}{\alpha}} + g_{F22}.$$

Substituting the above inequality and

inequality (33) into Eq. (27) yields

$$\begin{aligned} \dot{V}_F \leq & -k_3 \sum_{i=1}^n \varsigma_i \sum_{j=0}^n a_{ij} \left(\varsigma_i^{\frac{1}{\alpha}} - \varsigma_j^{\frac{1}{\alpha}} \right) + \gamma_2 \\ & \cdot \sum_{i=1}^n \bar{v}_{T_i}^{2-\frac{1}{\alpha}} (u_{T_i} + \Delta_{T_i}) + (c_{\sigma 1} + c_{\sigma 2}) \sum_{i=1}^n |\varsigma_i|^{1+\frac{1}{\alpha}} \\ & + (c_{vT1} + c_{vT2}) \sum_{i=1}^n \bar{v}_{T_i}^{1+\frac{1}{\alpha}} + g_{F1} + g_{F22}, \end{aligned} \tag{40}$$

which makes the choices such that

$$u_{T_i} = -\Delta_{T_i} - k_4 \bar{v}_{T_i}^{\frac{2}{\alpha}-1}, \tag{41}$$

where the control gain k_4 will be set later. As a result, the closed-loop formation subsystem for the i^{th} follower is

$$\begin{cases} \dot{\varsigma}_i = -k_3 \sum_{j=0}^n a_{ij} \left(\varsigma_i^{\frac{1}{\alpha}} - \varsigma_j^{\frac{1}{\alpha}} \right) + \sum_{j=0}^n a_{ij} \\ \quad \cdot \left(\Delta_{\xi_i} - \Delta_{\xi_j} \right) + \sum_{j=0}^n a_{ij} \left(\frac{\partial \xi_i}{\partial s_i} \tilde{v}_{T_i} - \frac{\partial \xi_j}{\partial s_j} \tilde{v}_{T_j} \right), \\ \dot{\tilde{v}}_{T_i} = -\alpha v_{T_i}^{\alpha-1} k_4 \bar{v}_{T_i}^{\frac{2}{\alpha}-1} - \dot{v}_{T_i}^{\alpha}. \end{cases} \tag{42}$$

Let $\varsigma = [\varsigma_1, \varsigma_2, \dots, \varsigma_n]$. Substituting $-k_3 \varsigma^T L_1 \varsigma^{\frac{1}{\alpha}} \leq -k_3 \rho_{L_1} \sum_{i=1}^n |\varsigma_i|^{1+\frac{1}{\alpha}}$ and Eq. (41) into inequality (40) yields

$$\begin{aligned} \dot{V}_F \leq & -(k_3 \rho_{L_1} - c_{\sigma 1} - c_{\sigma 2}) \sum_{i=1}^n |\varsigma_i|^{1+\frac{1}{\alpha}} + g_{F1} \\ & - (k_4 \gamma_2 - c_{vT1} - c_{vT2}) \sum_{i=1}^n \bar{v}_{T_i}^{1+\frac{1}{\alpha}} + g_{F22}, \end{aligned}$$

in which control gains are chosen as follows:

$$\begin{cases} k_3 \geq \rho_{L_1}^{-1} (c_{\sigma 1} + c_{\sigma 2} + \beta_{F1}), \\ k_4 \geq \left(2 - \frac{1}{\alpha} \right) k_3^{1+\alpha} (c_{vT1} + c_{vT2} + \beta_{F1}), \end{cases} \tag{43}$$

where β_{F1} is an arbitrary positive constant. As a result, we have

$$\dot{V}_F \leq -\beta_{F1} \sum_{i=1}^n |\varsigma_i|^{1+\frac{1}{\alpha}} - \beta_{F1} \sum_{i=1}^n \bar{v}_{T_i}^{1+\frac{1}{\alpha}} + g_{F1} + g_{F22}. \tag{44}$$

Let $l_F = \max \left\{ 1, \frac{2^{1-\frac{1}{\alpha}}}{(2-\frac{1}{\alpha})k_3^{1+\alpha}} \right\}$. Then we have

$$V_F \leq l_F \sum_{i=1}^n (\varsigma_i^2 + \bar{v}_{T_i}^2), \tag{45}$$

which yields $V_F^{(1+\frac{1}{\alpha})/2} \leq l_F^{(1+\frac{1}{\alpha})/2} \left(\sum_{i=1}^n \varsigma_i^{1+\frac{1}{\alpha}} + \sum_{i=1}^n \bar{v}_{T_i}^{1+\frac{1}{\alpha}} \right)$. Suppose that $V_F(t) \neq 0$. Inequality (44) can be rewritten as

$$\dot{V}_F \leq -\beta_{F2} V_F^{(1+\frac{1}{\alpha})/2} + g_{F3}, \tag{46}$$

where $\beta_{F2} = \beta_{F1}/l_F^{(1+\frac{1}{\alpha})/2}$ and $g_{F3} = g_{F1} + g_{F22}$. Due to $0 < (1 + \frac{1}{\alpha})/2 < 1$, β_{F2} has a lower bound. g_{F3} approaches zero as $\lim_{t \rightarrow T} \lambda_i(t) = 0$ and $\lim_{t \rightarrow T} \bar{v}_{N_i}(t) = 0$, as proved in Theorem 1. We give the following result directly:

Theorem 2 Suppose that the initial positions of vehicles are such that $p_i(0) \in \Omega_i$. Assume moreover that Assumption 1 holds. Then the formation objective (Eq. (7)) can be achieved by the finite-time control u_{T_i} given in Eq. (41), for $i = 1, 2, \dots, n$.

Proof The proof follows the same argument as the proof of Theorem 5.3 in Bhat and Bernstein (2000) (which is provided in the supplementary materials). Hence, it is omitted.

Theorems 1 and 2 yield the following result:

Theorem 3 Suppose that the initial positions of vehicles are such that $p_i(0) \in \Omega_i$. Assume moreover that Assumption 1 holds. For $i = 1, 2, \dots, n$, the finite-time coordinated path-following control problem is solved by the coordinated path-following control:

$$u_i = \begin{bmatrix} N_i^T \\ T_i^T \end{bmatrix}^{-1} \begin{bmatrix} u_{N_i} \\ u_{T_i} \end{bmatrix}, \tag{47}$$

where u_{N_i} and u_{T_i} are as given in Eqs. (19) and (41), respectively.

Remark 5 Different from the consensus problem studied in Li SH et al. (2011), this study addresses the coordinated path-following control problem, which includes two subproblems, i.e., path-following and formation control. Moreover, the digraph in this paper, assumed to consist of a virtual leader and n vehicles, contains a directed spanning tree with root \mathcal{V}_0 , while in Li SH et al. (2011), each follower was required to access to the leader's states.

Now, let us consider a special case: the virtual leader has a velocity $\dot{\xi}_0 = \eta_0$ along the responding orbit and its velocity accesses to each follower, where η_0 and $\dot{\eta}_0$ are bounded signals. In this case, the open-loop equations of the path-following subsystem are Eqs. (8) and (9), which are the same as those of the static case. Let $\tilde{\xi}_i = \xi_i - \xi_0$. The time derivative of $\tilde{\xi}_i$ is $\dot{\tilde{\xi}}_i = \frac{\partial \xi_i}{\partial s_i} \tilde{v}_{T_i} + \Delta_{\xi_i}$,

where $\tilde{v}_{T_i} = v_{T_i} - \left(\frac{\partial \xi_i}{\partial s_i}\right)^{-1} \eta_0$. Differentiating both sides of \tilde{v}_{T_i} yields $\dot{\tilde{v}}_{T_i} = u_{T_i} + \tilde{\Delta}_{T_i}$, where $\tilde{\Delta}_{T_i} = \Delta_{T_i} - \left(\frac{\partial \xi_i}{\partial s_i}\right)^{-1} \dot{\eta}_0$. Let $\tilde{\zeta}_i = \sum_{j=1}^n a_{ij} (\tilde{\xi}_i - \tilde{\xi}_j)$ be the formation errors. The dynamics of $\tilde{\zeta}_i$ is

$$\dot{\tilde{\zeta}}_i = \sum_{j=1}^n a_{ij} \left(\frac{\partial \xi_i}{\partial s_i} \tilde{v}_{T_i} + \Delta_{\xi_i} - \frac{\partial \xi_j}{\partial s_j} \tilde{v}_{T_j} - \Delta_{\xi_j} \right), \quad (48)$$

which is similar to Eq. (12). As a result, the expressions of \tilde{v}_{N_i} and \tilde{u}_{N_i} are the same as Eqs. (13) and (19) in the static case, respectively. The expressions of \tilde{v}_{T_i} and \tilde{u}_{T_i} are also the same as Eqs. (25) and (41), respectively, in the static case by replacing ζ_i and Δ_{T_i} with $\tilde{\zeta}_i$ and $\tilde{\Delta}_{T_i}$, respectively.

We now give the following corollary directly:

Corollary 1 Consider that a virtual leader has a velocity η_0 along the responding orbit and that the access to each follower has been considered. Suppose that the initial vehicle positions are such that $p_i(0) \in \Omega_i$. For $i = 1, 2, \dots, n$, the finite-time coordinated path-following control problem is solved by the coordinated path-following control law (47), where u_{N_i} and u_{T_i} are as given in Eqs. (19) and (41), respectively.

4 Simulations

In this section, we first apply the proposed control laws in Theorem 3 to coordinate the vehicles moving along the elliptic orbits with a triangle pattern in case 1, and then use the control algorithm proposed in Corollary 1 to achieve the in-line formation in case 2. The selected trajectories of the agents are concentric ellipses with a different semi-major axis and semi-minor axis, that is, $C_{l0} : \frac{p_{x_l}^2}{(e_l a)^2} + \frac{p_{y_l}^2}{(e_l b)^2} = 1$, where $e_l = 1 + 0.5l$, $a = 3$, $b = 2$, and $l = 0, 1, 2, 3, 4$.

1. Case 1: static virtual leader

The topology for the virtual leader and followers is shown in Fig. 2. The parameters are selected as $k_1 = k_3 = 2.7$, $k_2 = k_4 = 34$, and $\alpha = \frac{9}{7}$. The initial generalized arc-length of the virtual leader is $\xi_0(0) = 0$. The motion of the agents is illustrated in Fig. 3, where “o”, “□”, “*”, and “+” denote the agents’ positions at $t = 0, 1, 2$, and 7 s, respectively. In this figure, one can see that the four followers converge to the given orbits and achieve the desired formation. The path-following errors λ_i and formation errors $\xi_i - \xi_0$ are plotted in Figs. 4 and 5, respec-

tively. The above figures show that path-following and formation tracking are achieved.

2. Case 2: dynamic virtual leader

We use the coordinated path-following control algorithm given in Corollary 1 to achieve the in-line pattern. The parameters are selected as $k_1 = k_2 = k_3 = k_4 = 10$ and $\alpha = \frac{5}{3}$. The motion of the agents, the path-following errors λ_i , and the formation errors $\xi_i - \xi_0$ are illustrated in Figs. 6, 7, and 8, respectively.

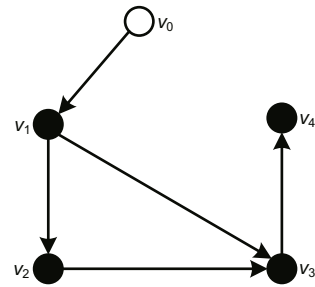


Fig. 2 A directed topology

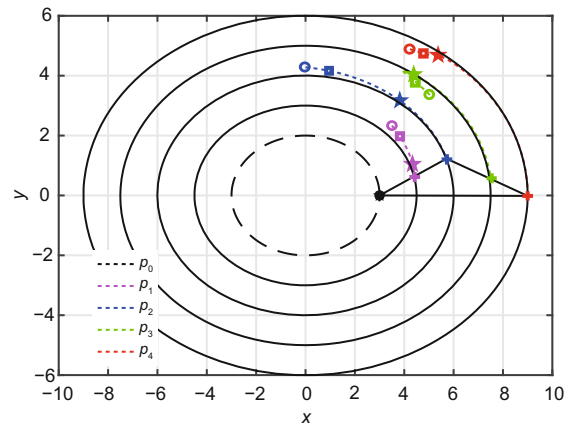


Fig. 3 Motion of the agents in the static virtual leader case

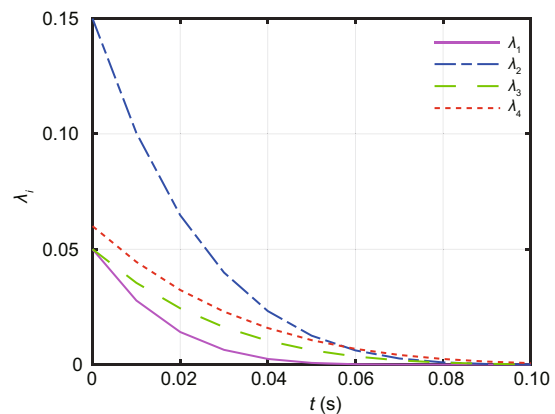


Fig. 4 Path-following errors in the static virtual leader case

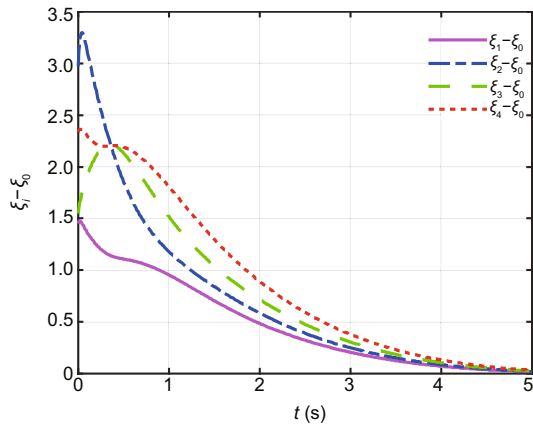


Fig. 5 Formation errors in the static virtual leader case

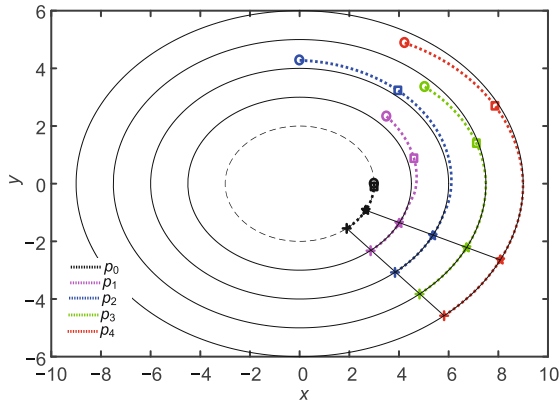


Fig. 6 Motion of the agents in the dynamic virtual leader case

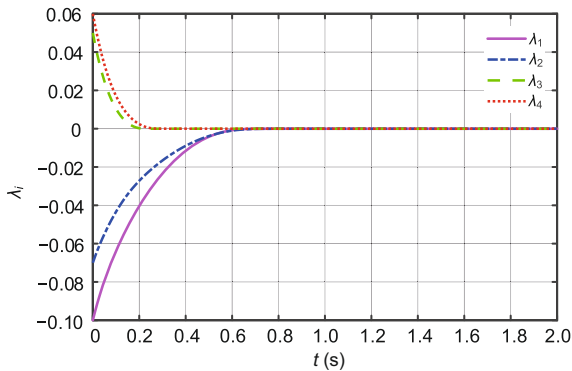


Fig. 7 Path-following errors in the dynamic virtual leader case

5 Conclusions

A continuous feedback method to solve the finite-time coordinated path-following control problem is presented, where the topology for the virtual leader and followers is directed. Because the movable ranges of the agents are restricted, a novel barrier function is given. A finite-time coordinated path-following control law in the static virtual leader case

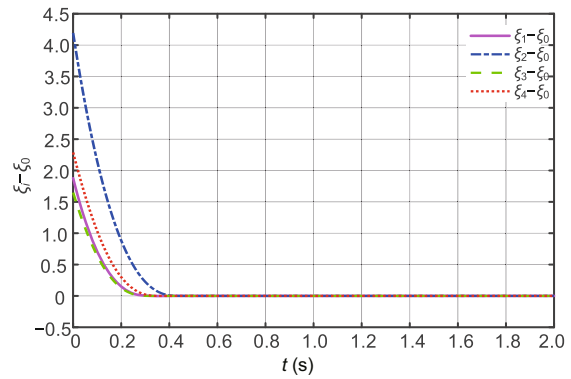


Fig. 8 Formation errors in the dynamic virtual leader case

is designed first. Then the control law is obtained in the dynamic virtual leader case, where its velocity can be accessed by each follower. Conditions on the control gains to guarantee that the path-following errors and the formation errors converge to zeros in finite time are presented. In ongoing work, the experiments involving finite-time coordinated path-following problems will be considered.

Contributors

Weibin CHEN designed the research. Yangyang CHEN drafted the paper. Ya ZHANG helped organize the paper. Weibin CHEN and Yangyang CHEN revised and finalized the paper.

Compliance with ethics guidelines

Weibin CHEN, Yangyang CHEN, and Ya ZHANG declare that they have no conflict of interest.

References

Bertozzi AL, Kemp M, Marthaler D, 2005. Determining environmental boundaries: asynchronous communication and physical scales. In: Kumar V, Leonard N, Morse AS (Eds.), Cooperative Control. Springer, Berlin, p.25-42. https://doi.org/10.1007/978-3-540-31595-7_2

Bhat SP, Bernstein DS, 2000. Finite-time stability of continuous autonomous systems. *SIAM J Contr Optim*, 38(3):751-766. <https://doi.org/10.1137/S0363012997321358>

Cao YC, Ren W, 2012. Distributed coordinated tracking with reduced interaction via a variable structure approach. *IEEE Trans Autom Contr*, 57(1):33-48. <https://doi.org/10.1109/TAC.2011.2146830>

Cao YC, Ren W, Li Y, 2009. Distributed discrete-time coordinated tracking with a time-varying reference state and limited communication. *Automatica*, 45(5):1299-1305. <https://doi.org/10.1016/j.automatica.2009.01.018>

Cao YC, Ren W, Meng ZY, 2010. Decentralized finite-time sliding mode estimators and their applications in decentralized finite-time formation tracking. *Syst Contr*

- Lett*, 59(9):522-529.
<https://doi.org/10.1016/j.sysconle.2010.06.002>
- Chen YY, Tian YP, 2015. Formation tracking and attitude synchronization control of underactuated ships along closed orbits. *Int J Robust Nonl Contr*, 25(16):3023-3044. <https://doi.org/10.1002/rnc.3246>
- Chen YY, Chen KW, Astolfi A, 2021a. Adaptive formation tracking control of directed networked vehicles in a time-varying flowfield. *J Guid Contr Dyn*, 44(10):1883-1891. <https://doi.org/10.2514/1.G005822>
- Chen YY, Chen KW, Astolfi A, 2021b. Adaptive formation tracking control for first-order agents in a time-varying flowfield. *IEEE Trans Autom Contr*, 67(5):2481-2488. <https://doi.org/10.1109/TAC.2021.3074900>
- Dou LQ, Yang C, Wang DD, et al., 2019. Distributed finite-time formation control for multiple quadrotors via local communications. *Int J Robust Nonl Contr*, 29(16):5588-5608. <https://doi.org/10.1002/rnc.4687>
- Du HB, Li SH, Lin XZ, 2013. Finite-time formation control of multiagent systems via dynamic output feedback. *Int J Robust Nonl Contr*, 23(14):1609-1628. <https://doi.org/10.1002/rnc.2849>
- Du HB, Wen GH, Cheng YY, et al., 2017. Distributed finite-time cooperative control of multiple high-order nonholonomic mobile robots. *IEEE Trans Neur Netw Learn Syst*, 28(12):2998-3006. <https://doi.org/10.1109/TNNLS.2016.2610140>
- Fiorelli E, Leonard NE, Bhatta P, et al., 2006. Multi-AUV control and adaptive sampling in Monterey bay. *IEEE J Oceanic Eng*, 31(4):935-948. <https://doi.org/10.1109/JOE.2006.880429>
- Ghabcheloo R, 2007. Coordinated Path Following of Multiple Autonomous Vehicles. PhD Dissertation, Universidade de Lisbon, Lisboa, Portugal.
- Guan ZH, Sun FL, Wang YW, et al., 2012. Finite-time consensus for leader-following second-order multi-agent networks. *IEEE Trans Circ Syst I Regul Pap*, 59(11):2646-2654. <https://doi.org/10.1109/TCSI.2012.2190676>
- Huang JS, Wen CY, Wang W, et al., 2015. Adaptive finite-time consensus control of a group of uncertain nonlinear mechanical systems. *Automatica*, 51:292-301. <https://doi.org/10.1016/j.automatica.2014.10.093>
- Khoo S, Xie LH, Man ZH, 2009. Robust finite-time consensus tracking algorithm for multirobot systems. *IEEE/ASME Trans Mechatron*, 14(2):219-228. <https://doi.org/10.1109/TMECH.2009.2014057>
- Li SH, Du HB, Lin XZ, 2011. Finite-time consensus algorithm for multi-agent systems with double-integrator dynamics. *Automatica*, 47(8):1706-1712. <https://doi.org/10.1016/j.automatica.2011.02.045>
- Li TS, Zhao R, Chen CLP, et al., 2018. Finite-time formation control of under-actuated ships using nonlinear sliding mode control. *IEEE Trans Cybern*, 48(11):3243-3253. <https://doi.org/10.1109/TCYB.2018.2794968>
- Peng ZH, Wang D, Chen ZY, et al., 2013. Adaptive dynamic surface control for formations of autonomous surface vehicles with uncertain dynamics. *IEEE Trans Contr Syst Technol*, 21(2):513-520. <https://doi.org/10.1109/TCST.2011.2181513>
- Qian CJ, Lin W, 2001. A continuous feedback approach to global strong stabilization of nonlinear systems. *IEEE Trans Autom Contr*, 46(7):1061-1079. <https://doi.org/10.1109/9.935058>
- Wang L, Xiao F, 2010. Finite-time consensus problems for networks of dynamic agents. *IEEE Trans Autom Contr*, 55(4):950-955. <https://doi.org/10.1109/TAC.2010.2041610>
- Wang N, Li H, 2020. Leader-follower formation control of surface vehicles: a fixed-time control approach. *ISA Trans*, 124(5):356-364. <https://doi.org/10.1016/j.isatra.2020.05.042>
- Xiao F, Wang L, Chen J, et al., 2009. Finite-time formation control for multi-agent systems. *Automatica*, 45(11):2605-2611. <https://doi.org/10.1016/j.automatica.2009.07.012>
- Yu JL, Dong XW, Li QD, et al., 2018. Practical time-varying formation tracking for second-order nonlinear multiagent systems with multiple leaders using adaptive neural networks. *IEEE Trans Neur Netw Learn Syst*, 29(12):6015-6025. <https://doi.org/10.1109/TNNLS.2018.2817880>
- Zhang FM, Leonard NE, 2007. Coordinated patterns of unit speed particles on a closed curve. *Syst Contr Lett*, 56(6):397-407. <https://doi.org/10.1016/j.sysconle.2006.10.027>
- Zhang FX, Chen YY, 2022. Finite-time tracking control for nonaffine nonlinear pure-feedback systems with a prescribed performance. *Int J Robust Nonl Contr*, 32(4):2212-2232. <https://doi.org/10.1002/rnc.5941>
- Zhang Y, Tian YP, 2009. Consentability and protocol design of multi-agent systems with stochastic switching topology. *Automatica*, 45(5):1195-1201. <https://doi.org/10.1016/j.automatica.2008.11.005>

List of electronic supplementary materials

- Theorem 4.2 in Bhat and Bernstein (2000)
- Theorem 5.3 in Bhat and Bernstein (2000)
- Proof of Eq. (10)
- Proof of inequality (15)
- Proof of inequality (16)
- Proof of inequality (18)
- Proof of Eq. (27)
- Proof of inequality (37)